Journal of Alloys and Compounds 504 (2010) 552–558

Contents lists available at ScienceDirect

Journal of Alloys and Compounds

journal homepage: www.elsevier.com/locate/jallcom

High temperature oxidation behavior of cobalt triantimonide thermoelectric material

Degang Zhao[a,*], Changwen Tian[a], Shouqiu Tang[a], Yunteng Liu[a], Lidong Chen[b]

[a] Institute of New Materials, Shandong Academy of Sciences, 19 Keyuan Road, Jinan, Shandong 250014, PR China
[b] Energy Materials Research Center, Shanghai Institute of Ceramics, Chinese Academy of Sciences, 1295 Dingxi Road, Shanghai 200050, PR China

ARTICLE INFO

Article history:
Received 22 March 2010
Received in revised form 20 May 2010
Accepted 29 May 2010
Available online 11 June 2010

Keywords:
Oxidation
Thermoelectric
$CoSb_3$

ABSTRACT

The oxidation behavior of $CoSb_3$ thermoelectric material in air has been studied from 500 °C to 650 °C. The present work showed that the growth of oxide scale on $CoSb_3$ material obeyed a parabolic law from 500 °C to 600 °C, while tremendous weight loss occurred at 650 °C owing to the sublimation of Sb_2O_3. The oxidation activation energy of $CoSb_3$ was estimated to be 37.4 kJ/mol. SEM and XRD results showed that the oxide scale of $CoSb_3$ was the mixture of Sb_2O_3 and $CoSb_2O_6$ when $CoSb_3$ was oxidized below 600 °C; whereas the oxide scale consisted of an outer layer of Sb_2O_3 and an inner layer, which was composed of Sb_2O_3 and $CoSb_2O_6$, when $CoSb_3$ was oxidized at 650 °C. Cracks appeared at the scale/$CoSb_3$ interface after a certain oxidation time. The oxidation mechanism of $CoSb_3$ material was discussed. After oxidation at 650 °C for 48 h, thermoelectric performance of $CoSb_3$ declined obviously and *ZT* value decreased from 0.24 to 0.17 at 327 °C.

1. Introduction

Thermoelectric (TE) conversion, as a reliable and static heat-to-electricity conversion technique, has attracted worldwide attention for the applications in electronic cooling, waste heat recovery and special power generation. Recently, thermoelectric generator (TEG) has been applied to the recovery of heat energy of combustible exhaust gas or waste water, because TEG system has a good flexibility to the heat source capacity and the change of temperature range. In general, the temperature of combustion gas in the solid waste incinerator changes from about 200 °C to 700 °C when the combustion gas flows from the burner to the bottom of chimney [1–3]. Because the conversion efficiency of TEG is in proportion to the hot junction temperature, it is better to equip the TEG at high temperature region.

There are many commercial TE materials, such as Bi_2Te_3, PbTe, $CoSb_3$, $FeSi_2$ and SiGe [4–7]. However, Bi_2Te_3 material is not suitable for industrial application when the temperature is higher than 250 °C and the conversion efficiency of $FeSi_2$ or SiGe is too low at the temperature range of 200–700 °C. PbTe material is harmful to human body and maybe causes environmental pollution. Doped or filled $CoSb_3$-based skutterudite compounds have high ZT value and are regarded as the promising materials working at intermediate temperature region [8,9]. Xiong et al. [10] fabricated the $Yb_{0.26}Co_4Sb_{12}$/GaSb nano-composite and achieved high thermoelectric performance, which resulted from the scattering of low-energy electrons by the GaSb-related boundary energy barriers. Li et al. [11] prepared the *n*-type skutterudite $In_xCe_yCo_4Sb_{12}$ with nano-structured InSb phase by melt-quench-anneal-spark plasma sintering method and *ZT* of 1.43 was achieved at 800 K. Vhitroub et al. [12] synthesized dual-element-doped skutterudite $Co_{23.87}Sb_{73.88}Pd_{1.125}Te_{1.125}$ by hot-pressed method and *ZT* value reached 1 at 873 K. Jiang et al. [13] prepared the $Sm_xCo_4Sb_{12}$ skutterudite compounds via the route of high pressure and high temperature and greatly improved the thermoelectric performance of $CoSb_3$. Therefore $CoSb_3$-based TEG is considered as the most suitable power generation system for many different industries. However, the oxidation of TE material at high temperature is an inevitable problem. Furthermore, the oxidation or sublimation of $CoSb_3$ at high temperature can result in the degradation of thermoelectric properties. Therefore, it is important to understand the oxidation behavior of $CoSb_3$ material in air. So far, few studies on the oxidation behavior of $CoSb_3$ were reported. Hara et al. [14,15] studied the surface oxidation of $CoSb_3$ and founded that two layers of oxidation products were formed; nevertheless the kinetic analysis and oxidation mechanism of $CoSb_3$ were not provided. Leszczynski et al. [16] compared the thermal oxidation behavior of $CoSb_3$ with that of CoP_3 and determined their starting temperatures of oxidation. In this study, we presented a detailed study on the oxidation behavior of $CoSb_3$ and reported some interesting results that had not been found in previous results. Related mechanism was atten-

* Corresponding author. Tel.: +86 531 88728308.
E-mail addresses: degangzhao@gmail.com, degang2008@163.com (D. Zhao).

0925-8388/$ – see front matter © 2010 Elsevier B.V. All rights reserved.
doi:10.1016/j.jallcom.2010.05.160

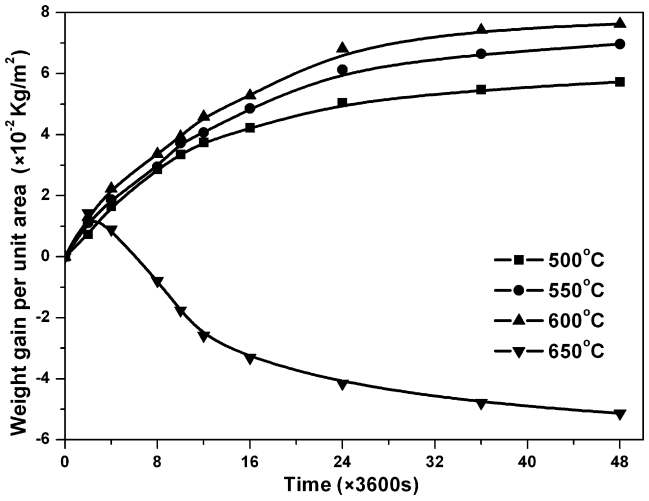

Fig. 1. Weight change per unit area as a function of time for $CoSb_3$ material from 500 °C to 650 °C.

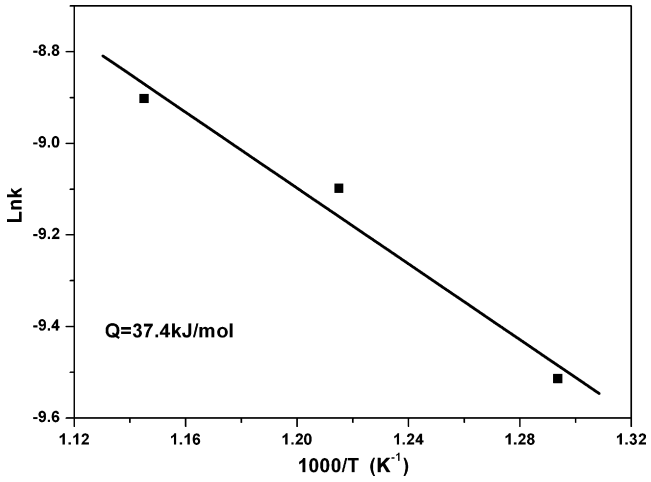

Fig. 2. Arrhenius plot of parabolic rate constant for oxidation of $CoSb_3$ from 500 °C to 600 °C.

tively discussed. The results are beneficial to the technological use of TEG.

2. Experimental procedures

The $CoSb_3$ ingots were prepared by melting the starting materials in vacuum-encapsulated quartz tube at 1080 °C followed by annealing at 600 °C for 150 h. The resulting ingots were ground into powder and then sintered in a graphite die by spark plasma sintering (SPS) in vacuum at 590 °C under a pressure of 50 MPa for 600 s. The samples with the dimensions of Ø10 × 3 mm were prepared from the sintered bulk $CoSb_3$. Both surfaces were metallographically polished down to 1 μm diamond paste and degreased in acetone before examination. The samples were heated at a rate of 200 °C/h in the furnace to the testing temperature (500–600 °C). After keeping at the testing temperature for desired time (0–48 h), the samples were cooled to room temperature in furnace naturally. The mass changes were calculated by the difference after and before the oxidation tests from an electronic balance with an accuracy of 0.1 mg. The oxidized surfaces of $CoSb_3$ samples were characterized by X-ray diffraction (XRD, Rigaku, Rint-2000) and scanning electron microscopy (SEM). The chemical composition of oxide scale was investigated by electron probe micro-analysis (EPMA, JEOL, JXA-8100) with an energy dispersive spectroscopy (EDS) system. Disc-type specimens with the dimensions of 10 mm (diameter) and 1 mm (thickness) were prepared for the test of thermal conductivity. Thermal conductivity was measured by a laser flash method (NETZSCH, LFA427) in vacuum. The Hall coefficient R_H was measured at room temperature with a constant magnetic field of 1 T. The carrier concentration n was determined using $n = 1/R_H e$, where e is the elementary electron charge. Parallelepiped specimens of dimensions 1.5 mm × 1.5 mm × 8 mm cut from the disc-shaped sample were used for the measurements of Seebeck coefficient and electrical conductivity, which were carried out by the standard four-probe method (ULVAC-RIKO, ZEM-2) in a flowing Ar atmosphere. All measurements were performed in the temperature range of 27–527 °C.

3. Results and discussion

3.1. Oxidation kinetics

Fig. 1 shows the weight change per unit area as a function of time in the temperature range from 500 °C to 650 °C in air for 48 h. It can be observed that the oxidation of $CoSb_3$ from 500 °C to 600 °C was in excellent agreement with a parabolic rate law. However, a tremendous weight loss occurred at 650 °C after 4 h of oxidation and then with the time prolonging, the weight loss proceeded. The results suggested that the oxidation mechanism of $CoSb_3$ material changed when the temperature increased from 600 °C to 650 °C. It maybe resulted from the sublimation of antimony or antimony oxide. The oxidation mechanism will be discussed in the latter part of the study.

Generally the weight gain of isothermal oxidation kinetics in the parabolic rule is expressed as by a rate equation:

$$(\Delta m)^2 = k_p \cdot t$$

where Δm is the weight gain per unit area, k_p the rate constant and t is the time [17,18]. And k_p follows an Arrhenius relation of the type:

$$k_p = k_0 \exp\left(-\frac{Q_{\text{eff}}}{RT}\right)$$

where Q_{eff} could be reflected by the slope coefficient from the Ln K versus $1/T$ plot during oxidation. After calculation, it was found that the parabolic rate constant (k_p) increased from 0.74×10^{-4} kg^2 m^{-4} s^{-1} at 500 °C to 1.36×10^{-4} kg^2 m^{-4} s^{-1} at 600 °C, which suggested $CoSb_3$ could be oxidized more intensively at higher temperature. The temperature dependence of the parabolic rate constants for $CoSb_3$ material from 500 °C to 600 °C is shown in Fig. 2. The oxidation activation energy of $CoSb_3$ was calculated to be 37.4 kJ/mol. The low activation energy meant that $CoSb_3$ was prone to be oxidized in air above 500 °C. It is also demonstrated that the coating or packaging of $CoSb_3$ is essential for industrial application.

3.2. Phase composition of oxide scales

The phase composition and surface morphology of the oxide surface were analyzed by X-ray diffraction and SEM. Fig. 3 shows the X-ray diffraction patterns of the oxide surface for $CoSb_3$ samples oxidized from 500 °C to 650 °C for 48 h. It can be noted that the oxides on the surface of $CoSb_3$, which formed at 500 °C, 550 °C and 600 °C, were mainly Sb_2O_3 and $CoSb_2O_6$; meanwhile, reflections from $CoSb_3$ were also observable, indicating the oxide scale was thin. However, it was strange that only reflections from Sb_2O_3 were observed at 650 °C. Fig. 4(a)–(d) show the surface morphology of the oxide scale of $CoSb_3$ oxidized in air from 500 °C to 650 °C for 48 h, respectively. It can be seen that the grain size of oxides increased with increasing temperature and different surface morphologies were also observed. Dense oxide scale, which was composed of bar-shaped crystallites and polyhedron crystallites, was observed for the sample oxidized at 500 °C, 550 °C and 600 °C. At 650 °C, however, the oxide scale of $CoSb_3$ material only consisted of large polyhedron crystallites with well-shaped facets. EDS analysis for the bar-shaped crystallites and polyhedron crystallites is presented in Fig. 5. The bar-shaped crystallites contained Sb, Co and O elements, while the polyhedron crystallites contained Sb and O elements. In consideration of the former XRD and EDS results, it was then concluded that the polyhedron crystallite was Sb_2O_3 phase. As for the case of bar-shaped crystallites materials, it should be $CoSb_2O_6$ phase.

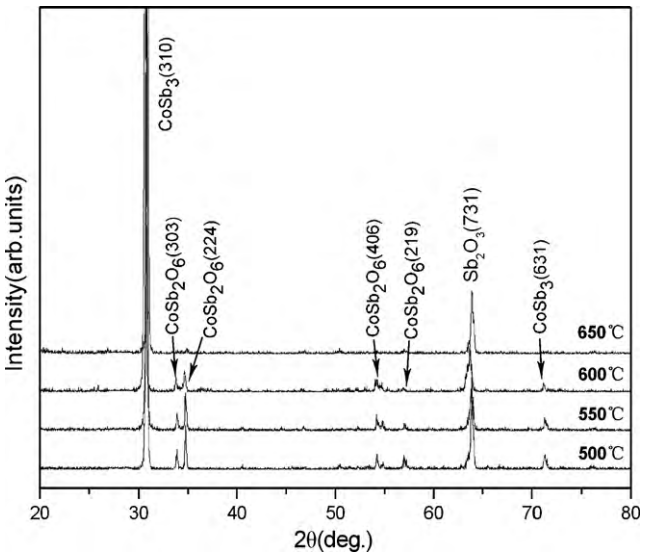

Fig. 3. X-ray diffraction patterns of the oxide surfaces on the $CoSb_3$ samples oxidized from 500 °C to 650 °C for 48 h.

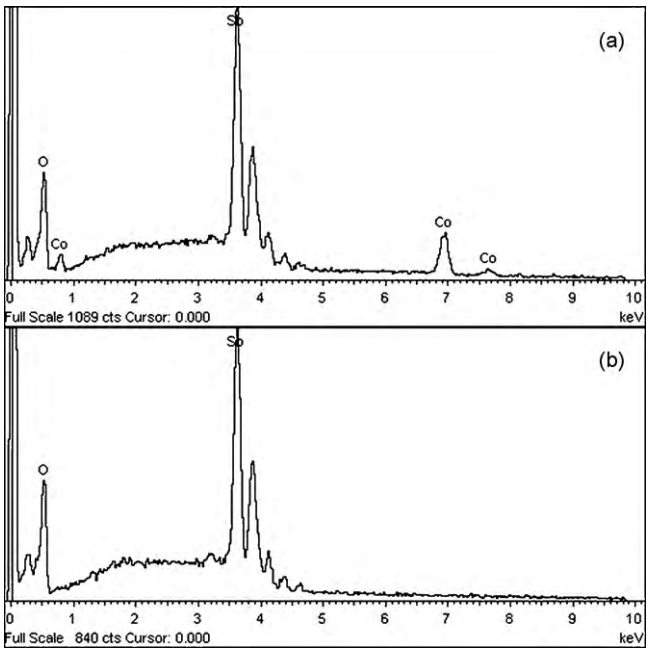

Fig. 5. EDS spectra for (a) bar-shaped crystallites and (b) large polyhedron crystallites in Fig. 4.

3.3. Morphology, structure and composition of sectioned samples

Fig. 6(a)–(c) show the SEM images of the cross-section of oxide scale after $CoSb_3$ sample was oxidized for different time at 600 °C. It can be seen that the oxide scale was one dark layer and with the oxidation time prolonging, the thickness of oxide scale increased. Fig. 7(a)–(d) are SEM image and EDX mapping of cross-section of $CoSb_3$ oxidized in air at 600 °C for 48 h. It can be observed that the dark oxide scale consisted of Sb, Co and O elements. With the help of EDS, the dark layer was analyzed to be composed of 13.76 at.% Co, 28.79 at.% Sb and 57.45 at.% O, as shown in Fig. 8(a), indicating the dark layer was the mixture of $CoSb_2O_6$ and Sb_2O_3 phase. Similar oxidation results were also observed on the $CoSb_3$ samples after oxidation at 500 °C and 550 °C. At 650 °C, however, the oxide layer contained two distinct parts, as shown in Fig. 6(d). According

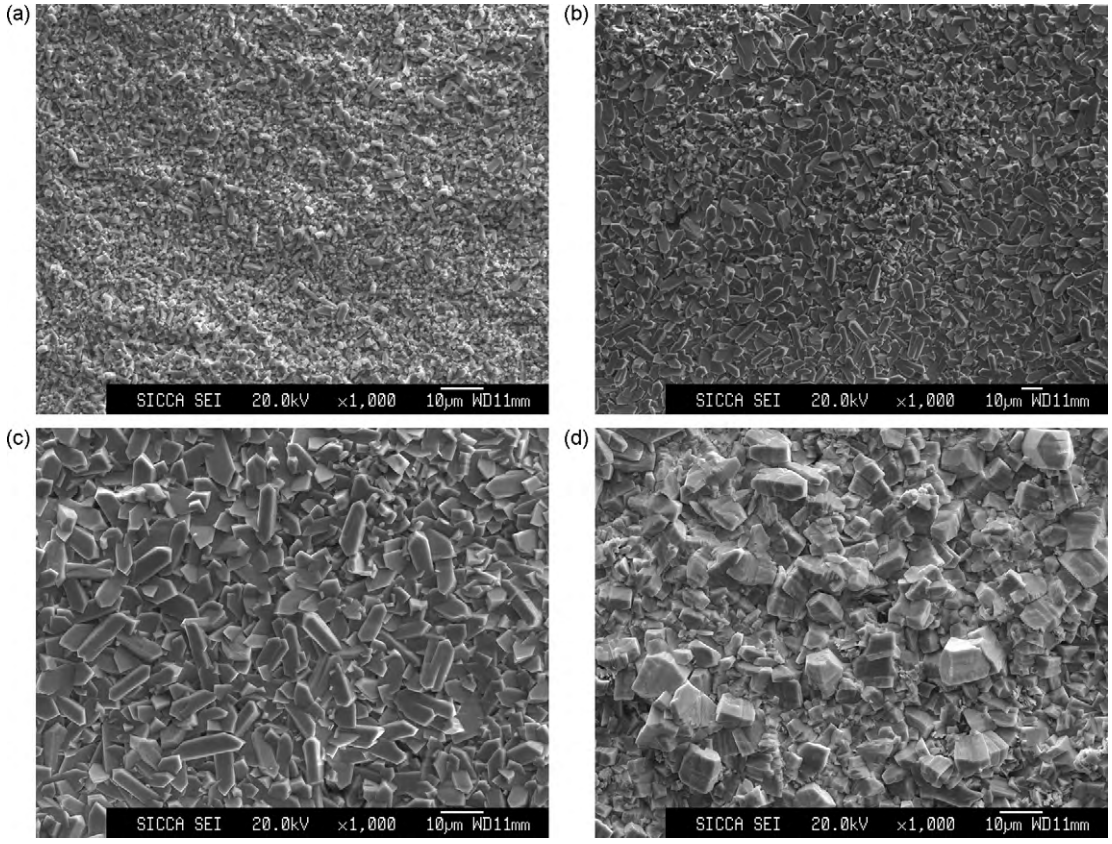

Fig. 4. Surface morphology of oxide scales after $CoSb_3$ exposure in air at different temperature for 48 h: (a) 500 °C; (b) 550 °C; (c) 600 °C; (d) 650 °C.

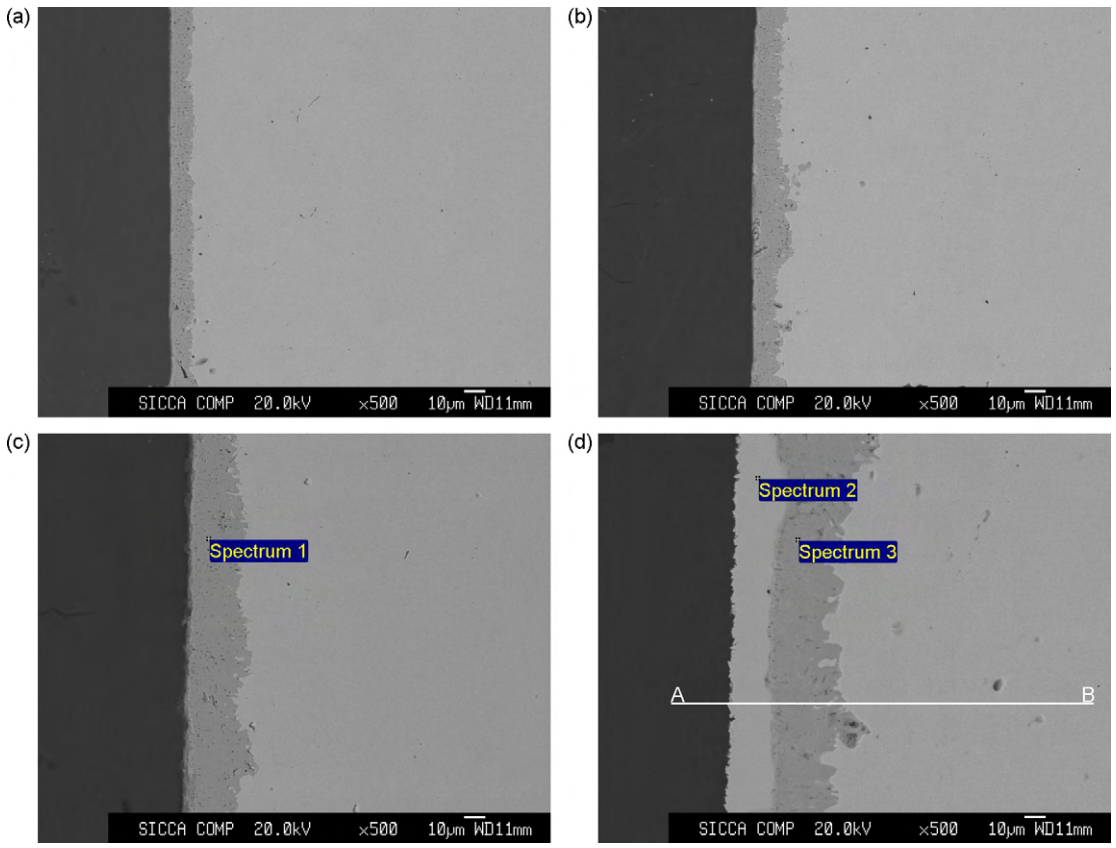

Fig. 6. SEM images of the cross-section of $CoSb_3$ oxidized in air: (a) 600 °C for 12 h; (b) 600 °C for 24 h; (c) 600 °C for 48 h; (d) 650 °C for 48 h.

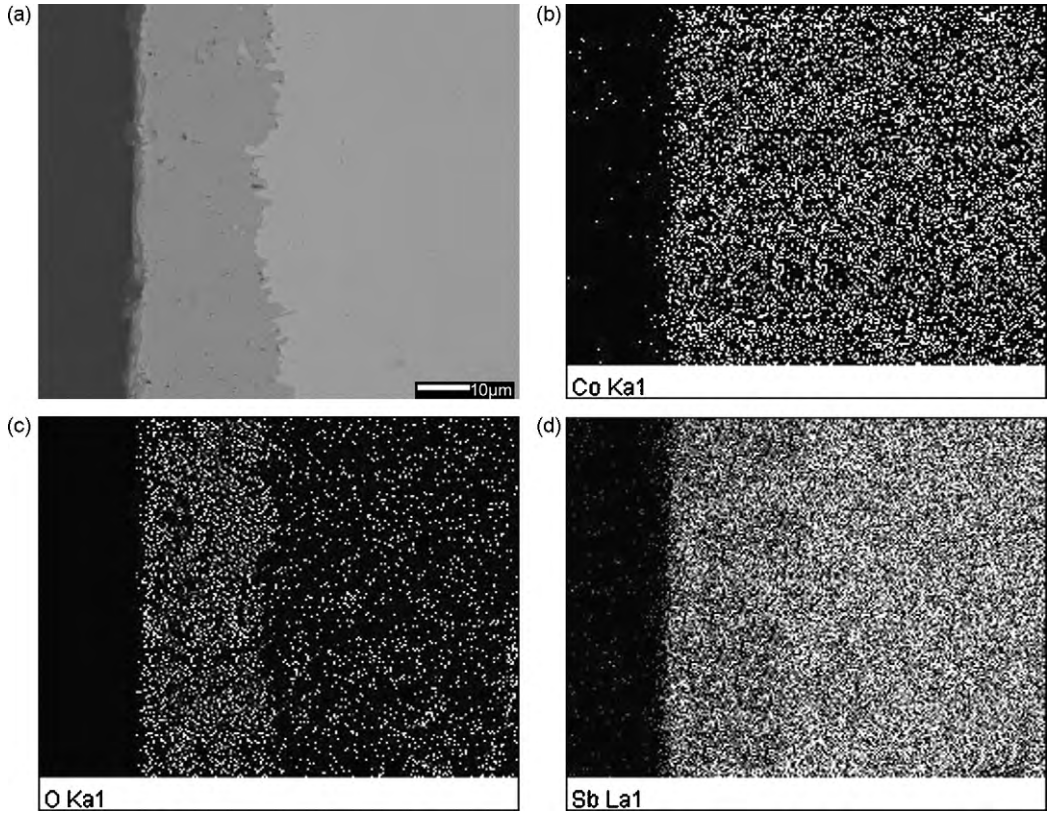

Fig. 7. SEM image and EDX mappings of cross-section of $CoSb_3$ oxidized in air at 600 °C for 48 h: (a) SEM micrograph; (b) Co; (c) O; (d) Sb.

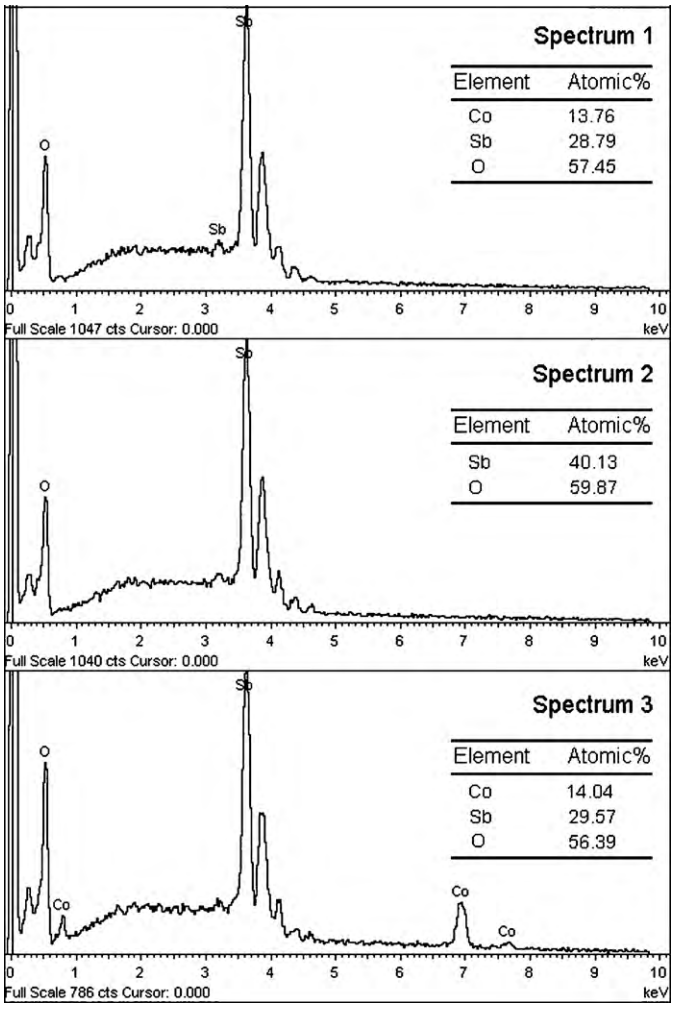

Fig. 8. EDS X-ray spectra in Fig. 6.

to the results of EDS, the outer layer was analyzed to be composed of 40.13 at.% Sb and 59.87 at.% O, corresponding to Sb_2O_3 phase; while the composition of inner layer was the same with the dark layer, as shown in Fig. 8(b) and (c). Fig. 9 shows the result of EPMA line profiles of the oxidized sample in Fig. 6(d) from point A to B. It

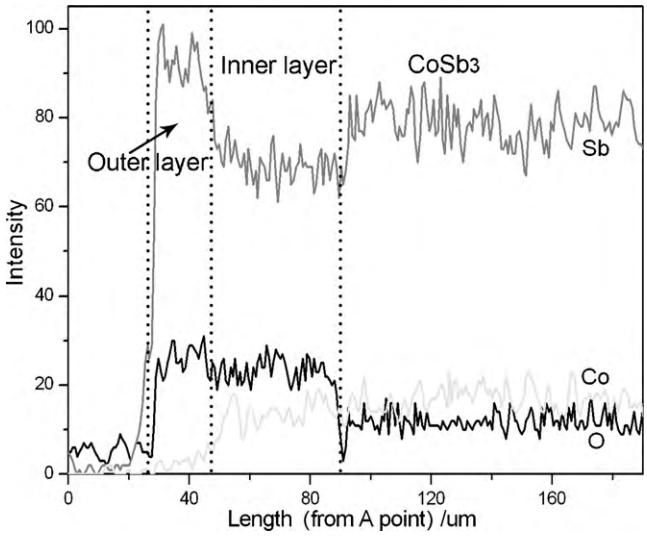

Fig. 9. EPMA line profiles from point A to B of $CoSb_3$ in Fig. 6.

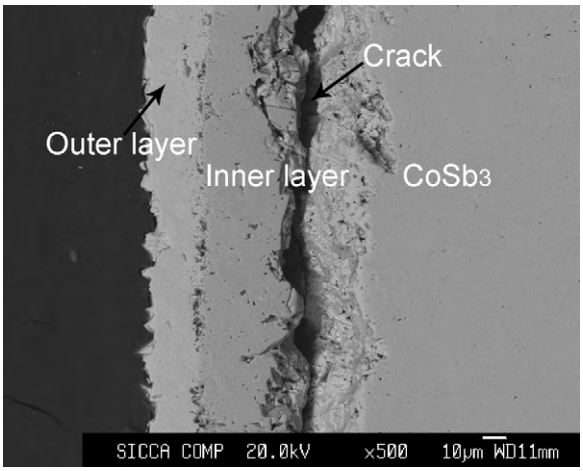

Fig. 10. SEM image of the cross-section of $CoSb_3$ oxidized in air at 650 °C for 72 h.

can be seen that the concentration of Sb and Co of inner layer was lower than that of $CoSb_3$ while the concentration of O of inner layer was higher than that of $CoSb_3$, indicating the concentration change agreed with the characteristic of the diffusion process. However, the Sb concentration of outer layer was higher than that of inner layer. Combined with the results of oxidation kinetics, it can be concluded that the weight loss at 650 °C resulted from the sublimation of Sb_2O_3.

3.4. Oxidation mechanism

In the oxidation process, the inward diffusion of O and the simultaneous outward diffusion of Sb and Co resulted in the formation of mixture layer (Sb_2O_3 and $CoSb_2O_6$). The oxidation process of $CoSb_3$ can be expressed as the following reaction equation:

$$4CoSb_3 + 15O_2(g) = 4CoSb_2O_6 + 2Sb_2O_3$$

So the thickness of dark layer increased with the oxidation time prolonging. However, when the temperature is above 600 °C, the sublimation reaction happens [19],

$$2Sb_2O_3(s) = Sb_4O_6(g)$$

Owing to the sublimation of Sb_2O_3 phase in the mixture layer, the concentration of Sb in the surface of oxide scale decreased which accelerated the outward diffusion of Sb. Moreover, Sb is easily to combine with oxygen to form Sb_2O_3 phase because of the large electrostatic attractive force between Sb^{3+} and O^{2-} [20]. When the rate of sublimation and the rate of diffusion struck a balance, the thickness of Sb_2O_3 layer would not change any longer. Therefore a two-layer scale formed after a certain oxidation time resulting from the sublimation of Sb_2O_3 phase. However, as the coefficient of thermal expansion of oxide scale is lower than that of $CoSb_3$, compressive stress generated at the scale/$CoSb_3$ interface when the temperature decreased. When the adherence of oxide scale could not stand the thermal stress, the cracks would appear and then the oxide scale detached from the $CoSb_3$ sample. Fig. 10 shows the SEM image of cross-section of $CoSb_3$ sample oxidized in air at 650 °C for 72 h. Similar cracks were also observed at the scale/$CoSb_3$ interface of $CoSb_3$ samples oxidized below 650 °C for 120 h. Cracks of the oxide scale could provide short-circuit diffusive channels of oxidation, therefore repetitive oxidation and detachment of oxide scale significantly decreased the TE properties of $CoSb_3$ and further degraded the TE performance of $CoSb_3$-based device.

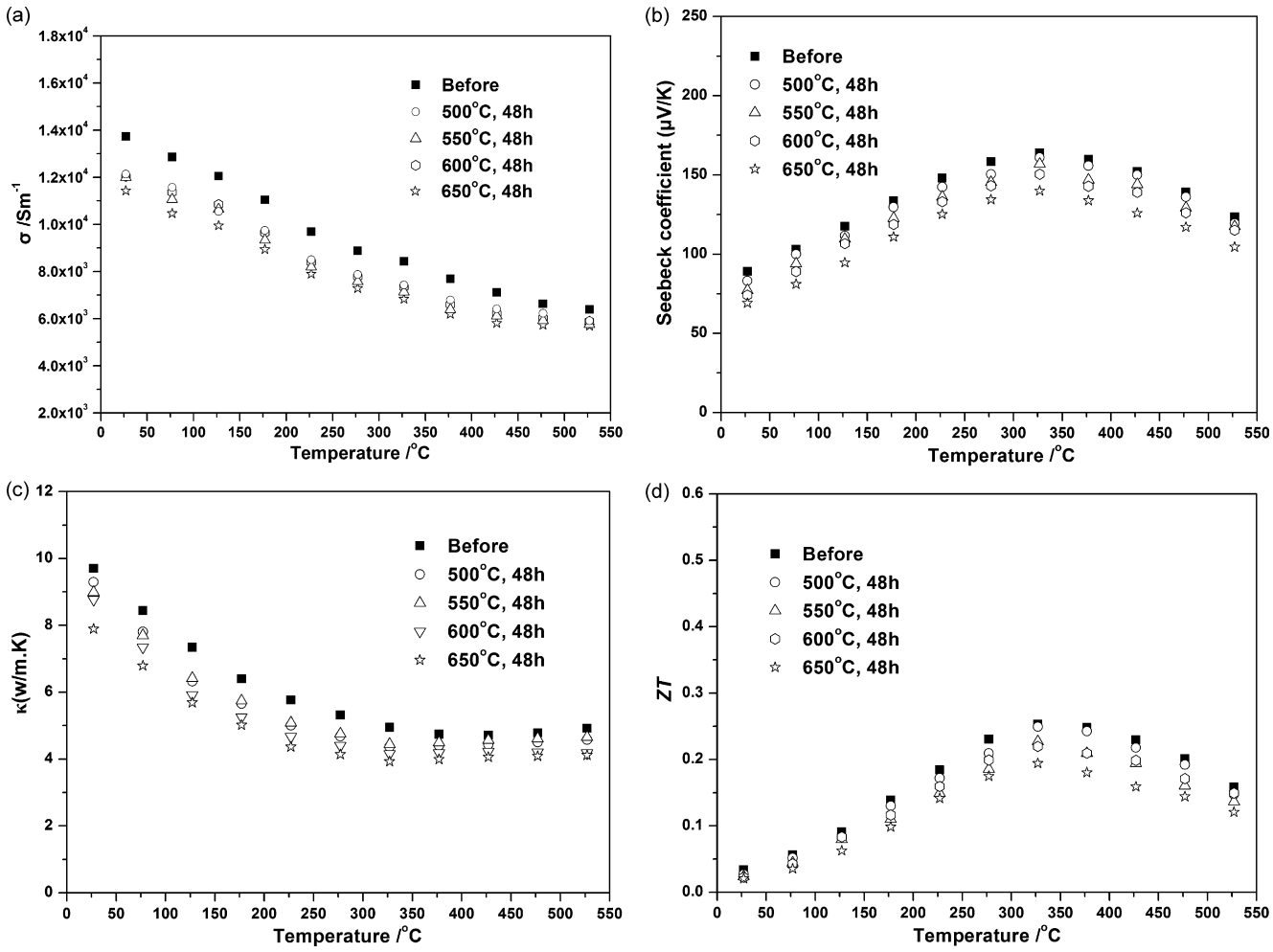

Fig. 11. Effect of oxidation on the thermoelectric properties of $CoSb_3$; (a) electrical conductivity; (b) Seebeck coefficient; (c) thermal conductivity; (d) *ZT*.

3.5. Thermoelectric properties

Fig. 11 shows the TE properties of $CoSb_3$ samples oxidized in air at different temperature for 48 h. The electrical conductivity declined evidently after oxidation at 650 °C for 48 h and the electrical conductivity at room temperature decreased by approximately 24%, as shown in Fig. 11(a). The carrier concentration of unoxidized $CoSb_3$ sample and oxidized sample (at 650 °C for 48 h) was $2.9 \times 10^{20}\,cm^{-3}$ and $2.2 \times 10^{20}\,cm^{-3}$, respectively. Therefore, the main reason for the decrease of electrical conductivity was the decline of carrier concentration resulting from the absence of Sb; the other was the formation of oxidation layer. Similar results have been founded in Hara's research [15]. Fig. 11(b) and (c) show the effects of oxidation on the Seebeck coefficient and thermal conductivity of $CoSb_3$ after oxidation at different temperature. The $CoSb_3$ was still P-type conductivity after oxidation. Because the electrical conductivity and thermal conductivity of the oxide scale were relatively small, the Seebeck coefficient and thermal conductivity of $CoSb_3$ samples declined to a certain degree. Due to the sublimation of Sb_2O_3 after oxidation at 650 °C, the density of sample decreased. Therefore the mean velocity of phone decreased, resulting in the decline of lattice thermal conductivity of $CoSb_3$. The conversion efficiency of TE materials depends on the maximum *ZT* values. Fig. 11(d) indicates the change of *ZT* value of $CoSb_3$ after high temperature oxidation. It can be seen that the *ZT* value of sample in the high temperature region significantly decreased and the *ZT* value decreased from 0.24 to 0.17 at 327 °C after oxidation at 650 °C for 48 h. The oxidation behavior of $CoSb_3$ and the degradation of TE properties put forward a new demand for the coating or package for $CoSb_3$ in the industrial application. The study about the coating for $CoSb_3$ will be carried out in future.

4. Conclusions

In this study, the oxidation behavior of $CoSb_3$ TE material in air from 500 °C to 650 °C was studied. The oxidation kinetics of $CoSb_3$ obeyed parabolic law below 600 °C; however, tremendous weight loss occurred at 650 °C owing to sublimation of Sb_2O_3. The oxide scale was the mixture of Sb_2O_3 and $CoSb_2O_6$ when $CoSb_3$ was oxidized below 600 °C; whereas it consisted of an outer layer of Sb_2O_3 and an inner layer, which was composed of Sb_2O_3 and $CoSb_2O_6$, when $CoSb_3$ was oxidized at 650 °C. With the oxidation time prolonging, the thickness of oxide scale and the grain size of oxide increased. After a certain oxidation time, cracks appeared at the scale/$CoSb_3$ interface and the oxide scale detached from $CoSb_3$ sample. After oxidation, TE performance of $CoSb_3$ decreased obviously, especially for the electrical conductivity. The *ZT* value of $CoSb_3$ significantly decreased in high temperature region.

Acknowledgements

This work is partly supported by National Basic Research Program of China Granted No. 2007CB607505, National High Technology Research and Development Program of China Granted No.

2007AA03Z233 and Key Project for Transformation of Independent Innovation Achievements of Shandong Province in China Granted No. 2009ZHZX1A0902.

References

[1] H. Scherrer, L. Vikhor, B. Lenoir, A. Dauscher, P. Poinas, J. Power. Sources 115 (2003) 141.
[2] R. Funahashi, M. Mikami, T. Mihare, S. Urata, N. Ando, J. Appl. Phys. 99 (2006) 066117.
[3] L. Zhang, A. Grytsiv, M. Kerber, P. Rogl, E. Bauer, M. Zehetbauer, J. Alloys Compd. 490 (2010) 19.
[4] G. Chen, M.S. Dresselhaus, G. Dresselhaus, J.-P. Fleurial, Int. Mater. Rev. 48 (2003) 1.
[5] S.B. Riffat, X. Ma, Appl. Therm. Eng. 23 (2003) 913.
[6] V.L. Kuznetsov, A.E. Kaliazin, D.M. Rowe, J. Mater. Sci. 37 (2002) 2893.
[7] J.L. Cui, X.B. Zhao, W.M. Zhao, Mat. Sci. Eng. B 94 (2002) 223.
[8] X. Shi, W. Zhang, L.D. Chen, J. Yang, C. Uher, Phys. Rev. B 75 (2007) 235208.
[9] S.Q. Bai, Y.Z. Pei, L.D. Chen, W.Q. Zhang, Acta Mater. 57 (2009) 3135.
[10] Z. Xiong, X.H. Chen, X.Y. Huang, S.Q. Bai, L.D. Chen, Acta Mater. 58 (2010) 3995.
[11] H. Li, X.F. Tang, Q.J. Zhang, C. Uher, Appl. Phys. Lett. 94 (2009) 102114.
[12] M. Chitroub, F. Besse, H. Scherrer, J. Alloys Compd. 467 (2009) 31.
[13] Y.P. Jiang, X.P. Jia, T.C. Su, N. Dong, F.R. Yu, J. Alloys Compd. 493 (2010) 535.
[14] R. Hara, S. Inoue, H.T. Kaibe, S. Sano, Proceedings of 20th International Conference on Thermoelectrics, IEEE, Beijing, China, 2001, p. 84.
[15] R. Hara, S. Inoue, H.T. Kaibe, S. Sano, J. Alloys Compd. 349 (2003) 297.
[16] J. Leszczynski, A. Malecki, K.T. Wojciechowski, Proceedings of 5th European Conference on Thermoelectrics, IEEE, Odessa, Ukraine, 2007, p. 50.
[17] X.M. Wang, W.D. Wu, Y.J. Tang, X.Q. Zeng, S.S. Yao, J. Alloys Compd. 474 (2009) 499.
[18] X.K. Qian, Y.B. Li, Y. Sun, X.D. He, C.C. Zhu, J. Alloys Compd. 491 (2010) 386.
[19] N.A. Asryan, A.S. Alikhanyan, G.D. Nipan, Dokl. Phys. Chem. 392 (2003) 201.
[20] D. Chatterji, J.V. Smith, J. Electrochem. Soc. 120 (1973) 889.